D. De Santis, G. Geraci, A. Guardone
Equivalence Conditions for the Finite Volume and Finite Element Methods in Spherical Coordinates
Mathematics and Computers in Simulation, Vol. 106, 2014, p. 60-75
doi:10.1016/j.matcom.2012.04.010

Equivalence Conditions for the Finite Volumes and Finite Elements Methods in Spherical Coordinates

D. De Santis[a], G. Geraci[a], A. Guardone[b,*]

[a] *INRIA Bordeaux–Sud-Ouest, 351 Cours de la Libration 33405 Talence, France*
[b] *Dipartimento di Ingegneria Aerospaziale, Politecnico di Milano, Via La Masa, 34, 20156 Milano, Italy*

Abstract

A numerical technique for the solution of the compressible flow equations over unstructured grids in a spherical reference is presented. The proposed approach is based on a mixed finite volume / finite element discretization in space. Equivalence conditions relating the finite volume and the finite element metrics in spherical coordinates are derived. Numerical simulations of the explosion and implosion problems for inviscid compressible flows are carried out to evaluate the correctness of the numerical scheme and compare fairly well to one-dimensional simulations over very fine grids.

Keywords: Compressible flows; Shock waves; Explosion/Implosion problem; Spherical coordinates; Finite Element/Volume methods.

1. Introduction

In a spherical reference, diverse gasdynamics problems exhibit relevant symmetries. These are, e.g., detonations, astrophysical flows, Inertial Confinement Fusion (ICF) applications, sonoluminescence phenomena and nuclear explosions [1]. To compute the numerical solution of the compressible flow equations for these kind of flows, an interesting possibility is provided by the use of a mixed finite volume (FV) / finite element (FE) approach [2]. For example, in viscous flows, it is possible to use the FV and the FE to compute the advection and dissipation terms, respectively, within the same algorithm [3, 4, 5]. The typical approach to build such methods is to evaluate the fluxes of the Euler equations by a classical stabilized node-centered FV scheme and to exploit the FE viewpoint to discretize the viscous or diffusion terms of the NavierStokes equations as well as to possibly estimate the solution gradients, needed by high order reconstruction schemes [6]. Such a possibility is expected to be of use in the study of the effect of viscosity on e.g. the formation of stable shock fronts and on the determination of the onset and dynamics of Richtmyer-Meshkov instabilities in spherical implosions [7].

The combined use of FV and FE techniques is made possible by the introduction of suitable equivalence conditions that relate the FV metrics, i.e. cell volumes and integrated normals, to the FE integrals. Equivalence conditions relating the two schemes have been derived for Cartesian coordinates in two and three spatial dimensions [6, 8] and for cylindrical coordinates in axially symmetric two-dimensional problems [9]. In both cited references, equivalence conditions are obtained by neglecting higher order FE contributions. Subsequently in [10], equivalence conditions for the cylindrical coordinates have been derived for the first time without introducing any approximation into the FE discrete expression of the divergence operator, and in [11] the difference between the consistent scheme and that violating the the equivalence conditions have been examined for the case of one-dimensional problems in cylindrical and spherical coordinates. In the present paper the consistent formulation between FV and FE is extended to the case of spherical coordinates r, θ, ϕ, with r, θ and ϕ, respectively, radial, polar and azimuthal coordinate.

The present paper is structured as follows. In section 2, the FE and FV schemes are briefly described for a scalar conservation law. Equivalence conditions are demonstrated in this case. The extension to the system of Euler equations

*Corresponding author
Email address: alberto.guardone@polimi.it (A. Guardone)

for compressible flow is also sketched. In section 3, numerical simulations are presented for the explosion and implosion problems in the spherical coordinates on the r–ϕ plane and are compared to one-dimensional simulations. In section 4 final remarks and comments are given.

2. Finite volume/element method in spherical coordinates

In the present section, the finite element and finite volume discrete equations for an exemplary scalar conservation law in a three-dimensional spherical reference are given. The model equation reads

$$\frac{\partial u}{\partial t} + \frac{1}{r^2}\frac{\partial}{\partial r}(r^2 f_r) + \frac{1}{r\sin\theta}\frac{\partial}{\partial\theta}(\sin\theta f_\theta) + \frac{1}{r\sin\theta}\frac{\partial f_\phi}{\partial\phi} = 0,$$

where t is the time, r, θ and ϕ are the radial, polar and azimuthal coordinates, respectively, $u = u(r, \theta, \phi, t)$ is the scalar unknown and $\boldsymbol{f}^\circ(u) = (f_r, f_\theta, f_\phi)$ is the so-called flux function. A more compact form of the above equation is obtained by introducing the divergence operator in three-dimensional spherical coordinates, $\boldsymbol{\nabla}^\circ\cdot(\cdot)$, as follows

$$\frac{\partial(u)}{\partial t} + \boldsymbol{\nabla}^\circ\cdot\boldsymbol{f}^\circ(u) = 0, \tag{1}$$

with

$$\boldsymbol{\nabla}^\circ\cdot\boldsymbol{f}^\circ(u) = \frac{2}{r}f_r + \frac{\partial f_r}{\partial r} + \frac{1}{r\sin\theta}\frac{\partial}{\partial\theta}(\sin\theta f_\theta) + \frac{1}{r\sin\theta}\frac{\partial f_\phi}{\partial\phi}$$

Equation (1) is first discretized in space by means of the FE and the FV method; equivalence conditions relating the two approaches are then derived. Finally, the numerical scheme is applied to the compressible Euler equations and time discretization is discussed.

2.1. Node-pair finite element discretization

The scalar conservation law (1) is first multiplied by the term $r\sin\theta$ to formally remove the singularity at the origin of the reference system, see [11]. The weak form of the resulting equation is obtained by multiplying the differential equation by test functions $\varphi \in V \subset H^1(\Omega)$ and integrating over the domain Ω as follows

$$\int_\Omega \varphi\, r\sin\theta\,\frac{\partial u}{\partial t}\,d\Omega^\circ + \int_\Omega \varphi\, r\sin\theta\,\boldsymbol{\nabla}^\circ\cdot\boldsymbol{f}^\circ(u)\,d\Omega^\circ,$$

to simplify the notation, the infinitesimal volume $d\Omega^\circ = r^2\sin\theta\,\mathrm{d}r\mathrm{d}\theta\mathrm{d}\phi$ will not be indicated in the integrals. An integration by parts gives

$$\int_\Omega \varphi\, r\sin\theta\,\frac{\partial u}{\partial t} = \int_\Omega \varphi\,\boldsymbol{f}^\circ(u)\cdot\boldsymbol{\nabla}^\circ(r\sin\theta) + \int_\Omega r\sin\theta\,\boldsymbol{f}^\circ(u)\cdot\boldsymbol{\nabla}^\circ\varphi - \oint_{\partial\Omega} r\sin\theta\,\varphi\,\boldsymbol{f}^\circ(u)\cdot\boldsymbol{n}^\circ,$$

where $\partial\Omega$ is the domain boundary and $\boldsymbol{n}^\circ = n_r\hat{\boldsymbol{r}} + n_\theta\hat{\boldsymbol{\theta}} + n_\phi\hat{\boldsymbol{\phi}}$ is the outward normal versor to Ω.

The discrete form of the above equation is obtained by considering a finite dimensional space $V_h \subset H^1$ of Lagrangian test functions φ_h, to obtain

$$\int_{\Omega_i}\varphi_i r\sin\theta\frac{\partial u}{\partial t} = \int_{\Omega_i}\varphi_i\,\boldsymbol{f}^\circ(u)\cdot\boldsymbol{\nabla}^\circ(r\sin\theta) + \int_{\Omega_i} r\sin\theta\boldsymbol{f}^\circ(u)\cdot\boldsymbol{\nabla}^\circ\varphi_i - \int_{\partial\Omega_i^\partial} r\sin\theta\varphi_i\,\boldsymbol{f}^\circ(u)\cdot\boldsymbol{n}^\circ, \quad \forall i \in \mathcal{N}$$

where $\mathcal{N}$ denotes the set of all nodes of the triangulations, Ω_i is the support of the basis function $\varphi_i \in V_h$ associated to node i and the shorthand notation $\partial\Omega_i^\partial = \partial\Omega_i \cap \partial\Omega$ was introduced. The scalar unknown is now interpolated by an expansion in the same space of the shape function as follows

$$u(r, \theta, \phi, t) \simeq u_h(r, \theta, \phi, t) = \sum_{k\in\mathcal{N}} u_k(t)\varphi_k(r, \theta, \phi),$$

to obtain the Bubnov-Galerkin approximation of (1) as

$$\sum_{k\in\mathcal{N}_i}\frac{du_k}{dt}M^{\circ}_{ik}=\int_{\Omega_i}r\sin\theta\boldsymbol{f}^{\circ}(u_h)\cdot\boldsymbol{\nabla}^{\circ}\varphi_i+\int_{\Omega_i}\varphi_i\boldsymbol{f}^{\circ}(u_h)\cdot\boldsymbol{\nabla}^{\circ}(r\sin\theta)-\int_{\partial\Omega_i^{\partial}}r\sin\theta\varphi_i\boldsymbol{f}^{\circ}(u_h)\cdot\boldsymbol{n}^{\circ},\tag{2}$$

where $\mathcal{N}_i$ is the set of shape functions φ_k whose support Ω_k overlaps Ω_i and where

$$M^{\circ}_{ik}\overset{\text{def}}{=}\int_{\Omega_{ik}}r\sin\theta\varphi_i\varphi_k\,d\Omega^{\circ},$$

with $\Omega_{ik}=\Omega_i\cap\Omega_k$. By resorting to the so-called flux interpolation technique [12], the flux function $\boldsymbol{f}^{\circ}(u_h)$ is now expanded using the same shape function $\varphi_h\in V_h$ as follows

$$\boldsymbol{f}^{\circ}(u_h(r,\theta,\phi,\,t))=\boldsymbol{f}^{\circ}\left(\sum_{k\in\mathcal{N}}u_k(t)\varphi_k(r,\theta,\phi)\right)\simeq\sum_{k\in\mathcal{N}}\boldsymbol{f}^{\circ}_k(t)\varphi_k(r,\theta,\phi),$$

where $\boldsymbol{f}^{\circ}_k(t)=\boldsymbol{f}^{\circ}(u_k(t))$, to obtain

$$\sum_{k\in\mathcal{N}_i}\frac{du_k}{dt}M^{\circ}_{ik}=\sum_{k\in\mathcal{N}_i}\boldsymbol{f}^{\circ}_k\cdot\int_{\Omega_{ik}}r\sin\theta\varphi_k\boldsymbol{\nabla}^{\circ}\varphi_i+\sum_{k\in\mathcal{N}_i}\boldsymbol{f}^{\circ}_k\cdot\int_{\Omega_{ik}}\varphi_i\varphi_k\boldsymbol{\nabla}^{\circ}(r\sin\theta)-\sum_{k\in\mathcal{N}_i}\boldsymbol{f}^{\circ}_k\cdot\int_{\partial\Omega^{\partial}_{ik}}r\sin\theta\varphi_i\varphi_k\boldsymbol{n}^{\circ},\tag{3}$$

where $\partial\Omega^{\partial}_{ik}=\partial\Omega_i\cap\partial\Omega_k\cap\partial\Omega$ and $\mathcal{N}_i^{\partial}$ is the set of all boundary nodes of Ω_i. Using the following identities

$$\begin{aligned}\sum_{k\in\mathcal{N}_i}\boldsymbol{f}^{\circ}_k\cdot\int_{\Omega_{ik}}r\sin\theta\varphi_k\boldsymbol{\nabla}^{\circ}\varphi_i&=\sum_{k\in\mathcal{N}_{i,\neq}}\left(\frac{\boldsymbol{f}^{\circ}_k+\boldsymbol{f}^{\circ}_i}{2}\cdot\boldsymbol{\eta}^{\circ}_{ik}-\frac{\boldsymbol{f}^{\circ}_k-\boldsymbol{f}^{\circ}_i}{2}\cdot\boldsymbol{\zeta}^{\circ}_{ik}\right)+\sum_{k\in\mathcal{N}_{i,\neq}}\frac{\boldsymbol{f}^{\circ}_k-\boldsymbol{f}^{\circ}_i}{2}\cdot\boldsymbol{\chi}^{\circ}_{ik},\\\sum_{k\in\mathcal{N}_i}\boldsymbol{f}^{\circ}_k\cdot\int_{\partial\Omega^{\partial}_{ik}}r\sin\theta\varphi_i\varphi_k\boldsymbol{n}^{\circ}&=\sum_{k\in\mathcal{N}^{\partial}_{i,\neq}}(\boldsymbol{f}^{\circ}_k-\boldsymbol{f}^{\circ}_i)\cdot\boldsymbol{\chi}^{\circ}_{ik}-\boldsymbol{f}^{\circ}_i\cdot\boldsymbol{\xi}^{\circ}_i,\end{aligned}$$

demonstrated in Appendix Appendix A, the node-pair representation of (3) is found to be

$$L^{\circ}_i\frac{du_i}{dt}=-\sum_{k\in\mathcal{N}_{i,\neq}}\left(\frac{\boldsymbol{f}^{\circ}_k+\boldsymbol{f}^{\circ}_i}{2}\cdot\boldsymbol{\eta}^{\circ}_{ik}-\frac{\boldsymbol{f}^{\circ}_k-\boldsymbol{f}^{\circ}_i}{2}\cdot\boldsymbol{\zeta}^{\circ}_{ik}\right)+\boldsymbol{f}^{\circ}_i\cdot\widehat{\boldsymbol{L}}^{\circ}_i-\sum_{k\in\mathcal{N}^{\partial}_{i,\neq}}\frac{\boldsymbol{f}^{\circ}_k-\boldsymbol{f}^{\circ}_i}{2}\cdot\boldsymbol{\chi}^{\circ}_{ik}-\boldsymbol{f}^{\circ}_i\cdot\boldsymbol{\xi}^{\circ}_i,\tag{4}$$

where $\mathcal{N}_{i,\neq}=\mathcal{N}\backslash\{i\}$ and $\mathcal{N}^{\partial}_{i,\neq}=\mathcal{N}^{\partial}\backslash\{i\}$. In the expression above the following FE metric quantities are introduced

$$\begin{aligned}&\boldsymbol{\eta}^{\circ}_{ik}\overset{\text{def}}{=}\int_{\Omega_{ik}}r\sin\theta(\varphi_i\boldsymbol{\nabla}^{\circ}\varphi_k-\varphi_k\boldsymbol{\nabla}^{\circ}\varphi_i)\,d\Omega^{\circ},\quad\boldsymbol{\zeta}^{\circ}_{ik}\overset{\text{def}}{=}\int_{\Omega_{ik}}\varphi_i\varphi_k\boldsymbol{\nabla}^{\circ}(r\sin\theta)\,d\Omega^{\circ},\quad\widehat{\boldsymbol{L}}^{\circ}_i\overset{\text{def}}{=}\int_{\Omega_{ik}}\varphi_i\boldsymbol{\nabla}^{\circ}(r\sin\theta)\,d\Omega^{\circ},\\&\boldsymbol{\chi}^{\circ}_{ik}\overset{\text{def}}{=}\int_{\partial\Omega^{\partial}_{ik}}r\sin\theta\varphi_i\varphi_k\boldsymbol{n}^{\circ}\,d\partial\Omega^{\circ},\qquad\qquad\boldsymbol{\xi}^{\circ}_i\overset{\text{def}}{=}\int_{\partial\Omega^{\partial}_{ik}}r\sin\theta\varphi_i\boldsymbol{n}^{\circ}\,d\partial\Omega^{\circ}.\end{aligned}\tag{5}$$

2.2. Edge-based finite volume discretization

The spatially discrete form of the scalar conservation law (1) is now obtained according to the node-centred finite volume approach [13]. To this purpose, the scalar conservation law (1) is multiplied by the quantity $r\sin\theta$ in written in integral form to obtain

$$\frac{d}{dt}\int_C u(r,\theta,\phi,\,t)=-\int_C\boldsymbol{\nabla}^{\circ}\cdot\boldsymbol{f}^{\circ}(u),\quad\forall C\subseteq\Omega,$$

by integrating by parts the right hand side and by applying the divergence theorem the above equation reads

$$\frac{d}{dt}\int_C u(r,\theta,\phi,\,t)=-\oint_C\boldsymbol{f}^{\circ}(u)\cdot\boldsymbol{n}^{\circ}+\int_C\boldsymbol{f}^{\circ}(u)\cdot\boldsymbol{\nabla}^{\circ}(r\sin\theta),$$

Its discrete counterpart is obtained by considering a certain number of finite volumes C_i , with boundary ∂C_i, each of them surrounding a single node i of the triangulation of Ω.

$$\frac{d}{dt}\int_{C_i} u(r,\theta,\phi,\,t) = -\oint_{\partial C_i} \boldsymbol{f}^{\circledcirc}(u)\cdot\boldsymbol{n}^{\circledcirc} + \int_{C} \boldsymbol{f}^{\circledcirc}(u)\cdot\boldsymbol{\nabla}^{\circledcirc}(r\sin\theta), \quad \forall i \in \mathcal{N}$$

The finite volumes C_i satisfy the following conditions

$$\begin{aligned} \mathring{C}_i \cap \mathring{C}_k &= \emptyset, \quad \forall i,k \in \mathcal{N}, i \neq k, \\ \bigcup_{k\in\mathcal{N}} C_k &= \Omega, \quad \forall i,k \in \mathcal{N}, i \neq k, \\ i \in C_i \Rightarrow i \notin C_k, &\quad \forall i,k \in \mathcal{N}, i \neq k. \end{aligned}$$

The first condition guarantees that the open sets $\mathring{C}_i$ are non-overlapping, the second condition assures that all the domain is covered by the finite volume, while the third condition implies that each finite volume C_i is associated with a single node i. Over each control volume C_i the cell-averaged unknown is introduced as follows

$$u(r,\theta,\phi,\,t) \simeq u_i = \frac{1}{V_i}\int_{C_i} u(r,\theta,\phi,\,t),$$

where V_i is the volume of the i-th cell. Therefore

$$V_i^{\circledcirc}\frac{du_i}{dt} = -\oint_{\partial C_i} r\sin\theta\, \boldsymbol{f}^{\circledcirc}\cdot\boldsymbol{n}^{\circledcirc} + \int_{C_i} \boldsymbol{f}^{\circledcirc}\cdot\boldsymbol{\nabla}^{\circledcirc}(r\sin\theta), \quad \text{where} \quad V_i^{\circledcirc} \overset{\text{def}}{=} \int_{C_i} r\sin\theta.$$

The boundary integral on the right hand side is now split into interface or edge contributions as follows

$$V_i^{\circledcirc}\frac{du_i}{dt} = -\sum_{k\in\mathcal{N}_{i,\neq}}\int_{\partial C_{ik}} r\sin\theta\,\boldsymbol{f}^{\circledcirc}\cdot\boldsymbol{n}_i^{\circledcirc} - \int_{\partial C_i^{\partial}} r\sin\theta\,\boldsymbol{f}^{\circledcirc}\cdot\boldsymbol{n}^{\circledcirc} + \int_{C_i}\boldsymbol{f}^{\circledcirc}\cdot\boldsymbol{\nabla}^{\circledcirc}(r\sin\theta)$$

where $\mathcal{N}_{i,\neq}$ is the set of the finite volume C_k sharing a boundary with C_i, excluding C_i and where $\partial C_{ik} = \partial C_i \backslash \partial C_k \neq \emptyset, k \neq i$ is the so-called cell interface. Due to the piecewise constant approximation chosen for u, the discrete unknown is discontinuous across ∂C_{ik}. Therefore a numerical flux $\boldsymbol{f}_{ik}^{\circledcirc}$ is introduced, representing an approximation of $\boldsymbol{f}^{\circledcirc}(u)$ at the cell interface ∂C_{ik}. As it is standard practice the numerical flux is assumed to be constant over the cell interface, namely

$$\begin{aligned} \int_{\partial C_{ik}} r\sin\theta\,\boldsymbol{f}\cdot\boldsymbol{n}_i^{\circledcirc} &\simeq \boldsymbol{f}_{ik}^{\circledcirc}\cdot\int_{\partial C_{ik}} r\sin\theta\,\boldsymbol{n}_i^{\circledcirc} = \boldsymbol{f}_{ik}^{\circledcirc}\cdot\boldsymbol{\nu}_{ik}^{\circledcirc} \quad \text{with} \quad \boldsymbol{\nu}_{ik}^{\circledcirc} \overset{\text{def}}{=} \int_{\partial C_{ik}} r\sin\theta\,\boldsymbol{n}_i^{\circledcirc} \\ \int_{\partial C_i^{\partial}} r\sin\theta\,\boldsymbol{f}\cdot\boldsymbol{n}_i^{\circledcirc} &\simeq \boldsymbol{f}_{i}^{\circledcirc}\cdot\int_{\partial C_i^{\partial}} r\sin\theta\,\boldsymbol{n}_i^{\circledcirc} = \boldsymbol{f}_{ik}^{\circledcirc}\cdot\boldsymbol{\nu}_{i}^{\circledcirc} \quad \text{with} \quad \boldsymbol{\nu}_{i}^{\circledcirc} \overset{\text{def}}{=} \int_{\partial C_i^{\partial}} r\sin\theta\,\boldsymbol{n}_i^{\circledcirc}. \end{aligned}$$

If the second-order centred approximation of the fluxes is considered, $\boldsymbol{f}_{ik}^{\circledcirc} = \frac{\boldsymbol{f}_i^{\circledcirc}+\boldsymbol{f}_k^{\circledcirc}}{2}$, the final form of the finite volume approximation of (1) reads,

$$V_i^{\circledcirc}\frac{du_i}{dt} = -\sum_{k\in\mathcal{N}_{i,\neq}}\frac{\boldsymbol{f}_i^{\circledcirc}+\boldsymbol{f}_k^{\circledcirc}}{2}\cdot\boldsymbol{\nu}_{ik}^{\circledcirc} + \boldsymbol{f}_i^{\circledcirc}\cdot\widehat{\boldsymbol{V}}_i^{\circledcirc} - \boldsymbol{f}_i^{\circledcirc}\cdot\boldsymbol{\nu}_i^{\circledcirc}, \quad \text{with} \quad \widehat{\boldsymbol{V}}_i^{\circledcirc} \overset{\text{def}}{=} \int_{\partial C_i^{\partial}}\boldsymbol{\nabla}^{\circledcirc}(r\sin\theta) \tag{6}$$

to be compared to the corresponding FE discretization (4).

2.3. Finite Element/Volume equivalence

The equivalence conditions relating the above FV metric quantities and the FE ones defined in the previous section are now derived. To this purpose, relevant properties of the FE and FV discretizations are briefly recalled.

Considering FE metric quantities first, from its definition the vector $\boldsymbol{\eta}_{ik}^{\circ}$ is asymmetric, namely,

$$\boldsymbol{\eta}_{ik}^{\circ} = -\boldsymbol{\eta}_{ki}^{\circ}, \tag{7}$$

which will be referred in the following as property FE-a. Property FE-b is obtained by noting that (see identity A.7)

$$\sum_{k\in\mathcal{N}_i} \left(\boldsymbol{\eta}_{ik}^{\circ} - \boldsymbol{\zeta}_{ik}^{\circ}\right) + \boldsymbol{\xi}_i^{\circ} = \mathbf{0},$$

which by the lumping $\widehat{\boldsymbol{L}}_i^{\circ} = \sum_{k\in\mathcal{N}_i} \boldsymbol{\zeta}_{ik}^{\circ}$ gives immediately

$$\widehat{\boldsymbol{L}}_i^{\circ} - \sum_{k\in\mathcal{N}_{i,\neq}} \boldsymbol{\eta}_{ik}^{\circ} = \boldsymbol{\xi}_i^{\circ}. \tag{8}$$

Property FE-c stems from the following identity

$$\int_{\Omega_i} r\sin\theta\varphi_i \boldsymbol{\nabla}^{\circ}\cdot\boldsymbol{x}^{\circ} = \int_{\Omega_i} 3r\sin\theta\varphi_i = 3L_i^{\circ},$$

where $\boldsymbol{x}^{\circ}$ is the position vector, i.e., $\boldsymbol{x}^{\circ} = r\,\hat{\boldsymbol{r}}(\theta,\phi)$. On the other hand, by integrating by parts, one also has

$$\int_{\Omega_i} r\sin\theta\varphi_i \boldsymbol{\nabla}^{\circ}\cdot\boldsymbol{x}^{\circ} = \int_{\partial\Omega_i^{\partial}} r\sin\theta\varphi_i \boldsymbol{x}^{\circ}\cdot\boldsymbol{n}_i^{\circ} - \int_{\Omega_i} \varphi_i \boldsymbol{x}^{\circ}\cdot\boldsymbol{\nabla}^{\circ}(r\sin\theta) - \int_{\Omega_i} r\sin\theta\boldsymbol{x}^{\circ}\cdot\boldsymbol{\nabla}^{\circ}\varphi_i,$$

By substituting the exact expansion $\boldsymbol{x}^{\circ} = \sum_{k\in\mathcal{N}_i} \boldsymbol{x}_k^{\circ}\varphi_k$, and by applying the the FE node-pair representation described in section 2.1, the previous equation can be written as

$$3L_i^{\circ} = \sum_{k\in\mathcal{N}_{i,\neq}} \left(\frac{\boldsymbol{x}_k^{\circ}+\boldsymbol{x}_i^{\circ}}{2}\cdot\boldsymbol{\eta}_{ik}^{\circ} - \frac{\boldsymbol{x}_k^{\circ}-\boldsymbol{x}_i^{\circ}}{2}\cdot\boldsymbol{\zeta}_{ik}^{\circ}\right) - \boldsymbol{x}_i^{\circ}\cdot\widehat{\boldsymbol{L}}_i^{\circ} + \sum_{k\in\mathcal{N}_{i,\neq}^{\partial}} \frac{\boldsymbol{f}_k^{\circ}-\boldsymbol{f}_i^{\circ}}{2}\cdot\boldsymbol{\chi}_{ik}^{\circ} + \boldsymbol{x}_i^{\circ}\cdot\boldsymbol{\xi}_i^{\circ}.$$

By substituting property FE-b in the above identity, one finally obtains property FE-c as

$$3L_i^{\circ} = \sum_{k\in\mathcal{N}_{i,\neq}} \left(\frac{\boldsymbol{x}_k^{\circ}+\boldsymbol{x}_i^{\circ}}{2}\cdot\boldsymbol{\eta}_{ik}^{\circ} - \frac{\boldsymbol{x}_k^{\circ}-\boldsymbol{x}_i^{\circ}}{2}\cdot\boldsymbol{\zeta}_{ik}^{\circ}\right) + \sum_{k\in\mathcal{N}_{i,\neq}^{\partial}} \frac{\boldsymbol{f}_k^{\circ}-\boldsymbol{f}_i^{\circ}}{2}\cdot\boldsymbol{\chi}_{ik}^{\circ}. \tag{9}$$

Considering now FV metric quantities, from the fact that $\boldsymbol{n}_i^{\circ} = -\boldsymbol{n}_k^{\circ}$ over ∂C_{ik}, property FV-a reads $\boldsymbol{\nu}_{ik}^{\circ} = -\boldsymbol{\nu}_{ki}^{\circ}$, which corresponds to the conservation property of the scheme. From the Gauss theorem, one also has

$$\int_{C_i} \boldsymbol{\nabla}^{\circ}(r\sin\theta) = \oint_{\partial C_i} r\sin\theta\boldsymbol{n}_i^{\circ}$$

which, from the definition of FV metric quantities, gives property FV-b as

$$\widehat{\boldsymbol{V}}_i^{\circ} = \sum_{k\in\mathcal{N}_{i,\neq}} \boldsymbol{\nu}_{ik}^{\circ} + \boldsymbol{\nu}_i^{\circ}.$$

Property FV-c is obtained by noting that

$$3V_i^{\circ} = \int_{C_i} r\sin\theta\boldsymbol{\nabla}^{\circ}\cdot\boldsymbol{x}^{\circ} = \oint_{\partial C_i} r\sin\theta\boldsymbol{x}^{\circ}\cdot\boldsymbol{n}_i^{\circ} - \int_{C_i} \boldsymbol{\nabla}^{\circ}(r\sin\theta)\cdot\boldsymbol{x}^{\circ}.$$

The right hand side of the previous equation is now computed by means of the FV discretization as described in section 2.2

$$3V_i^{\circ} = \sum_{k\in\mathcal{N}_{i,\neq}} \frac{\boldsymbol{x}_i^{\circ}+\boldsymbol{x}_k^{\circ}}{2}\cdot\boldsymbol{\nu}_{ik}^{\circ} - \boldsymbol{x}_i^{\circ}\cdot\widehat{\boldsymbol{V}}_i^{\circ} + \boldsymbol{x}_i^{\circ}\cdot\boldsymbol{\nu}_i^{\circ},$$

inserting the property FV-b in the previous relation, the property FV-c is obtained as

$$3V_i^\circ = \sum_{k\in\mathcal{N}_{i,\neq}} \frac{\boldsymbol{x}_i^\circ + \boldsymbol{x}_k^\circ}{2} \cdot \boldsymbol{\nu}_{ik}^\circ. \tag{10}$$

Therefore, a FV approximation can be formally obtained from FE metric quantities defined over the same grid points by setting (see properties FE/FV-a and -b)

$$\boldsymbol{\nu}_{ik}^\circ = \boldsymbol{\eta}_{ik}^\circ, \quad \boldsymbol{\nu}_i^\circ = \boldsymbol{\xi}_i^\circ, \quad \widehat{\boldsymbol{V}}_i^\circ = \widehat{\boldsymbol{L}}_i^\circ.$$

Note that the mass lumping approximation $\sum_{k\in\mathcal{N}_i} M_{ik}^\circ \simeq L_i^\circ$, must be introduced in (4) for the equivalence conditions to be applicable. By subtracting (9) to (10), one finally has

$$V_i^\circ = L_i^\circ + \sum_{k\in\mathcal{N}_{i,\neq}} \frac{\boldsymbol{x}_k^\circ - \boldsymbol{x}_i^\circ}{6} \cdot \boldsymbol{\xi}_{ik}^\circ - \sum_{k\in\mathcal{N}_{i,\neq}^\partial} \frac{\boldsymbol{x}_k^\circ - \boldsymbol{x}_i^\circ}{6} \cdot \boldsymbol{\chi}_{ik}^\circ \tag{11}$$

It is remarkable that differently from the Cartesian case [6, 8], in the spherical reference, as well as in the cylindrical reference [10], the FV cell is not coincident with the FE lumped mass matrix. Moreover, the shape of the FV cells that guarantees equivalence with FE discretization still remains to be determined. The equivalence conditions allowed us to link the metrics of the FV scheme to the FE integrals. It is possible now to construct an hybrid scheme in which the FV and FE scheme can be combined to discretized the advective and diffusive terms, respectively, in a consistent manner. In the next section is reported a FV scheme for the Euler equation in which the metrics are computed directly from the FE integrals.

2.4. Fully discrete form of the Euler equations in spherical coordinates

The Euler equations in spherical coordinates for compressible inviscid flows are now briefly recalled. The differential form reads

$$\frac{\partial \mathbf{u}^\circ}{\partial t} + \boldsymbol{\nabla}^\circ \cdot \mathbf{f}^\circ = \frac{\boldsymbol{s}^\circ}{r\sin\theta} \tag{12}$$

where $\mathbf{u}^\circ(r,\theta,\phi,\,t) = (\rho, \boldsymbol{m}^\circ, E^t)^{\mathrm{T}}$ is the vector unknown of the density ρ, momentum vector $\boldsymbol{m}^\circ = (m_r, m_\theta, m_\phi)^{\mathrm{T}}$ and total energy per unit volume E^t; $\mathbf{f}^\circ$ is the flux function of the Euler equations in a spherical reference, defined as

$$\mathbf{f}^\circ(\mathbf{u}^\circ) = \begin{pmatrix} m_r & m_\theta & m_\phi \\ \frac{m_r^2}{\rho} + \Pi & \frac{m_\theta m_r}{\rho} & \frac{m_\phi m_r}{\rho} \\ \frac{m_r m_\theta}{\rho} & \frac{m_\theta^2}{\rho} + \Pi & \frac{m_\phi m_\theta}{\rho} \\ \frac{m_r m_\phi}{\rho} & \frac{m_\theta m_\phi}{\rho} & \frac{m_\phi^2}{\rho} + \Pi \\ \frac{m_r}{\rho}(E^t + \Pi) & \frac{m_\theta}{\rho}(E^t + \Pi) & \frac{m_\phi}{\rho}(E^t + \Pi) \end{pmatrix},$$

and $\boldsymbol{s}^\circ$ is the matrix of the source term, defined as

$$\boldsymbol{s}^\circ(\mathbf{u}^\circ) = \begin{pmatrix} 0 \\ \left(\frac{m_\theta^2}{\rho} + \Pi\right) + \left(\frac{m_\phi^2}{\rho} + \Pi\right) \\ -\frac{m_\theta m_r}{\rho} \\ -\frac{m_\phi m_r}{\rho} \\ 0 \end{pmatrix} \sin\theta + \begin{pmatrix} 0 \\ 0 \\ \frac{m_\phi^2}{\rho} + \Pi \\ -\frac{m_\phi m_\theta}{\rho} \\ 0 \end{pmatrix} \cos\theta = \breve{\boldsymbol{s}}^\circ \sin\theta + \overline{\boldsymbol{s}}^\circ \cos\theta,$$

with $\Pi(\mathbf{u}^\circ)$ the pressure function in terms of the conservative variables. For a polytropic, i.e., constant specific heats, ideal gas the pressure function reads

$$\Pi(\mathbf{u}^\circ) = (\gamma - 1)\left(E^t - \frac{|\boldsymbol{m}^\circ|^2}{2\rho}\right),$$

where γ is the ratio of the specific heats at constant pressure and volume. By introducing the FE approximation of the unknown $\mathbf{u}^\circ$ and the reinterpolation of the flux function $\mathbf{f}^\circ$ and of the source terms $\check{\boldsymbol{s}}^\circ, \overline{\boldsymbol{s}}^\circ$, namely

$$\mathbf{u}^\circ \simeq \sum_{k\in\mathcal{N}} \mathbf{u}_k^\circ(t)\,\varphi_k(r,\theta,\phi), \qquad \mathbf{f}^\circ(\mathbf{u}^\circ) \simeq \sum_{k\in\mathcal{N}} \mathbf{f}_k^\circ(t)\,\varphi_k(r,\theta,\phi),$$
$$\check{\boldsymbol{s}}^\circ(\mathbf{u}^\circ) \simeq \sum_{k\in\mathcal{N}} \check{\boldsymbol{s}}_k^\circ(t)\,\varphi_k(r,\theta,\phi), \qquad \overline{\boldsymbol{s}}^\circ(\mathbf{u}^\circ) \simeq \sum_{k\in\mathcal{N}} \overline{\boldsymbol{s}}_k^\circ(t)\,\varphi_k(r,\theta,\phi),$$

according to the procedures detailed in section (2.1) in the case of a scalar conservation law, the node-pair centered lumped FE approximation of the Euler equations (12) is immediately obtained as follows

$$L_i^\circ \frac{d\mathbf{u}_i^\circ}{dt} = -\sum_{k\in\mathcal{N}_i,\neq}\left(\frac{\mathbf{f}_k^\circ + \mathbf{f}_i^\circ}{2}\cdot\boldsymbol{\eta}_{ik}^\circ - \frac{\mathbf{f}_k^\circ - \mathbf{f}_i^\circ}{2}\cdot\boldsymbol{\zeta}_{ik}^\circ\right) + \mathbf{f}_i^\circ\cdot\widehat{\boldsymbol{L}}_i^\circ - \sum_{k\in\mathcal{N}_{i,\neq}^\partial}\frac{\mathbf{f}_k^\circ - \mathbf{f}_i^\circ}{2}\cdot\boldsymbol{\chi}_{ik}^\circ - \mathbf{f}_i^\circ\cdot\boldsymbol{\xi}_i^\circ + \check{\boldsymbol{s}}^\circ\check{L}_i + \overline{\boldsymbol{s}}^\circ\check{L}_i,$$

with the FE metric quantities defined in (5) and where

$$\check{L}_i = \sum_{k\in\mathcal{N}_i}\int_{\Omega_{ik}} r\sin^2\theta\varphi_i\varphi_k, \qquad \bar{L}_i = \sum_{k\in\mathcal{N}_i}\int_{\Omega_{ik}} r\sin\theta\cos\theta\varphi_i\varphi_k.$$

The corresponding FV discretization of the Euler equations is given by

$$V_i^\circ \frac{d\mathbf{u}_i^\circ}{dt} = -\sum_{k\in\mathcal{N}_{i,\neq}}\frac{\mathbf{f}_i^\circ + \mathbf{f}_k^\circ}{2}\cdot\boldsymbol{\eta}_{ik}^\circ + \boldsymbol{f}_i^\circ\cdot\widehat{\boldsymbol{L}}_i^\circ - \boldsymbol{f}_i^\circ\cdot\boldsymbol{\xi}_i^\circ + \check{\boldsymbol{s}}_i^\circ\hat{L}_i + \overline{\boldsymbol{s}}_i^\circ\check{L}_i,$$

where V_i° is computed from the equivalence condition (11). In the computation, a TVD [14] numerical flux is used, with the van Leer limiter [15]. The fully discrete form of the Euler system is obtained by a two-step Backward Differencing Formula. At each time level, a dual time-stepping technique is used to solve the time-implicit problem [16].

3. Numerical Results

In the present section, numerical results for converging and diverging spherical shock waves are presented in the two-dimension case, i.e. r-ϕ plane, and the results are compared against the solutions of the one-dimensional scheme [11].

The case of the explosion problem is considered first. The computational domain consists of a circular region with radius L. Initial conditions are as follows. The velocity is assumed to be zero everywhere; the density is uniform and equal to 1, whereas the pressure is ten times greater than its value in the outer zone only in a circular region centred at the origin with radius $L/2$. The perturbed state is indicated as state 1, while the unperturbed state is indicated as state 2, namely,

$$\rho(r) = \rho_1 \quad \forall r, \quad \boldsymbol{u}(r) = \mathbf{0} \quad \forall r, \quad P(r) = \begin{cases} P_1 & \text{for} \quad r \le L/2 \\ P_2 & \text{for} \quad r > L/2 \end{cases}$$

where $\boldsymbol{u}$ is the fluid velocity. The thermodynamic variables are made dimensionless by the values of the unperturbed zone and lengths are made dimensionless by the radius of the computational domain as follows

$$\bar{\rho} = \rho\bar{\rho}_2, \quad \bar{P} = P\bar{P}_2, \quad \bar{r} = r\bar{L}, \quad \bar{t} = t\bar{L}\sqrt{\bar{\rho}_2/\bar{P}_2}, \quad \bar{\boldsymbol{u}} = \boldsymbol{u}\sqrt{\bar{P}_2/\bar{\rho}_2},$$

where the overbar indicates dimensional variables and $\bar{L}$ is the unit reference length. In all computations, the ideal gas model for nitrogen ($\gamma = c_P/c_v = 1.39$) is used. The computational domain is shown in figure 1, where a representative

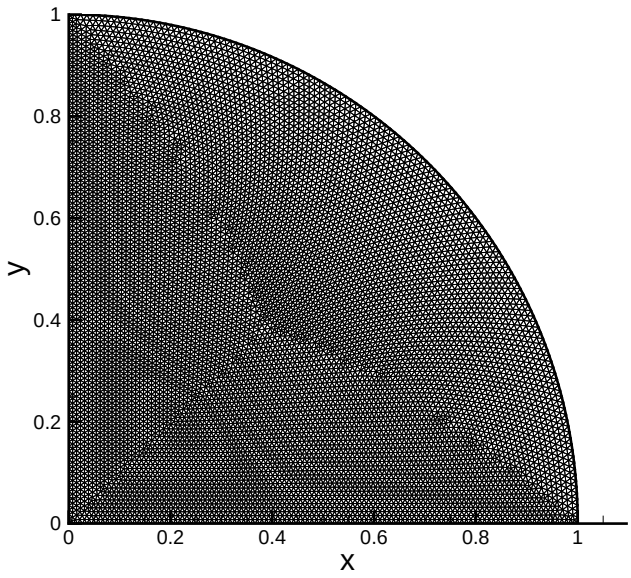

Figure 1: Exemplary grid for the explosion and implosion problems. The grid is the coarse one, see Table 1.

mesh	Nodes	Triangles	Resolution
Coarse	9 551	18 745	0.01
Medium	20 683	40 841	0.007
Fine	39 153	77 587	0.005

Table 1: Properties of the grids used in all the bidimensional simulations.

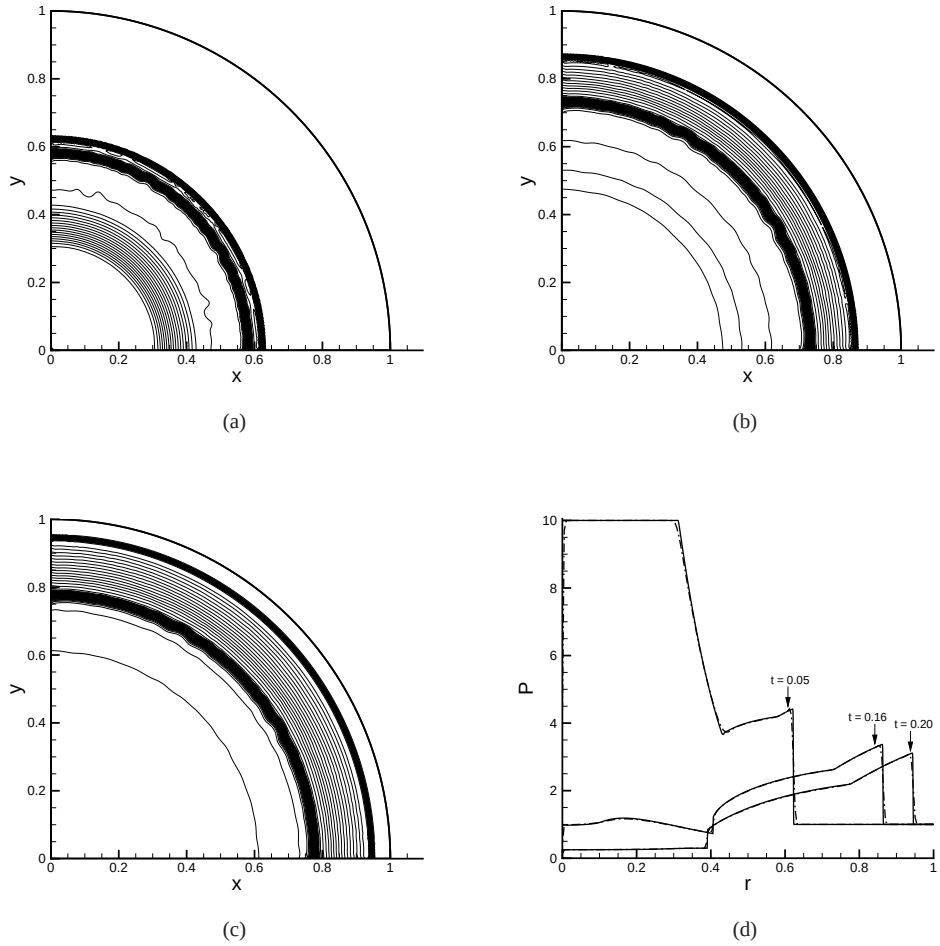

Figure 2: Density isoline for the explosion problem: (a) $t = 0.05$; (b) $t = 0.16$; (c) $t = 0.20$. Each isoline corresponds to a density difference of $\Delta\rho/\rho_{ref} = 0.03$. (d) Pressure signal along the $y = 0$ axis at the same time levels: the solid line is the reference one-dimensional solutions, the dot-dashed line is the bidimensional solution.

computational grid is also show. All the meshes employed are unstructured isotropic grids of Delaunay type generated by the means of the advancing front method of Rebay [17]. In all the simulations the wall-slip boundary conditions are applied to the boundaries of the computational domain. In table 1 are reported the properties of the different grid used to perform the simulations. In figure 2(a)–(c) density isolines at different time levels are shown for the explosion problem. The grid used in the computation shown is the fine one and the time step is $\Delta t = 1.5 \times 10^{-4}$. A spherical shock wave propagates towards the outer boundary of the computational domain; the shock wave is followed by a contact discontinuity. A rarefaction wave propagates towards the origin and is then reflected outward. Note that the initial corrugation of the shock front, due to the un-even shape of the initial discontinuity caused by its discrete representation over an unstructured grid of triangles, is clearly visible also at later times. In figure 2(d) the pressure signal along the $y = 0$ axis is compared against the reference one-dimensional results for three different time levels. The one-dimensional computation was performed over a evenly-spaced grid made of 2 001 nodes, which corresponds to an element spacing of 5×10^{-4}. A grid dependence study is shown in figure 3(a). Pressure signals along the $y = 0$ axis are compared at time $t = 0.16$ for the three different grid resolutions, numerical results are find to be almost independent from the grid resolution. Time step dependence can be appreciated from figure 3(b), where the pressure

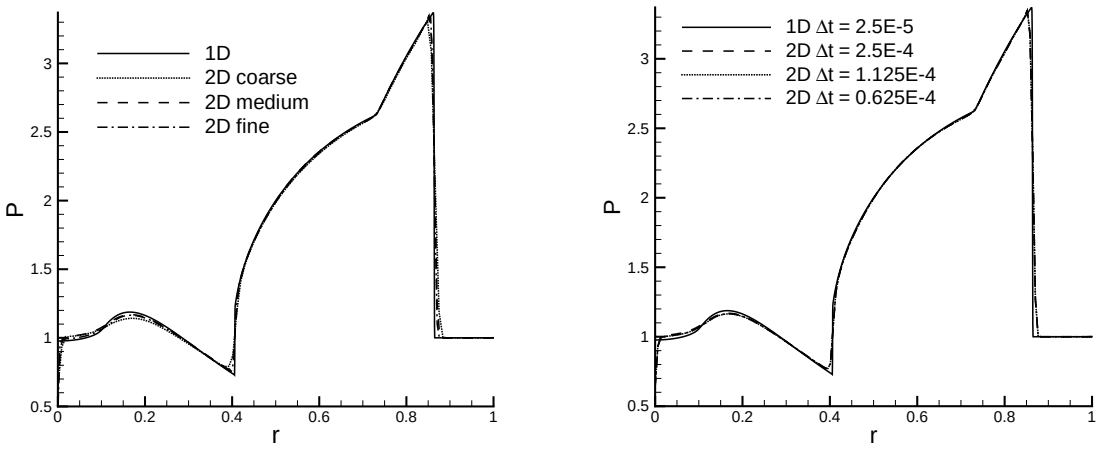

(a) (b)

Figure 3: Comparison of the pressure signal along the $y = 0$ axis for the explosion problem at time level $t = 0.16$ for grids with different space resolution (a), and for different time steps (b). The signal is compared against the reference one-dimensional solution.

signals for three different time steps is shown at time $t = 0.16$ for the medium grid. Numerical results are found to be independent from the chosen time step. In all computations, the solution at the grid node located at the origin of the reference system suffers from a significant undershoot, which however does not propagate inside the domain and does not affect the correct propagation of the reflected waves. In figure 4, numerical results for the implosion problem are shown. The initial condition is as in the explosion problem, where now the high pressure region is the outer one and the low pressure region is at $r \leq L/2$. The grid is the fine grid and the time step is 1.5×10^{-4}. A rarefaction wave propagates towards the outer boundary; a shock wave and a contact surface propagates inwards. The intensity of the shock increases as it moves towards the origin; when the shock wave is reflected at the origin, a region of high pressure/temperature is observed. Due to the symmetry of the solution and of the computational domain, the spherical implosion and explosion problems can be also simulated by axially symmetric Euler equations formulated in a cylindrical coordinate system, as done in [10]. The spherical and axisymmetric solution correspond to the solution of the same problem on two different planes, i.e., the r-ϕ plane in the spherical problem and the Z-R plane in the axisymmetric problem, where Z is the coordinate along the axis of symmetry and R is the coordinate along the axis normal to the axis of symmetry. The solutions in spherical coordinates are shown together with the corresponding solutions in axisymmetric coordinates in figure 5 for the explosion problem and in figure 6 for the implosion problem. In order to reconstruct the complete spherical solution the spherical and axisymmetric solutions are represented each on the corresponding plane.

4. Conclusions

A novel unstructured-grid hybrid finite element/volume method in a spherical reference was presented. The proposed approach represents an extension to the the spherical coordinates system of the node-pair scheme developed recently for the cylindrical case and earlier for the Cartesian one and moves from suitable equivalence conditions linking finite element integrals to the corresponding finite volume metrics, such as the cell volume or the integrated normals. The equivalence conditions were derived here without introducing any approximation and allowed to determine all needed finite volume metric quantities from finite element ones. This technique opens the way to mixed FV/FE formulation, in which the advective terms are computed by the means of the TVD FV approach and the FE

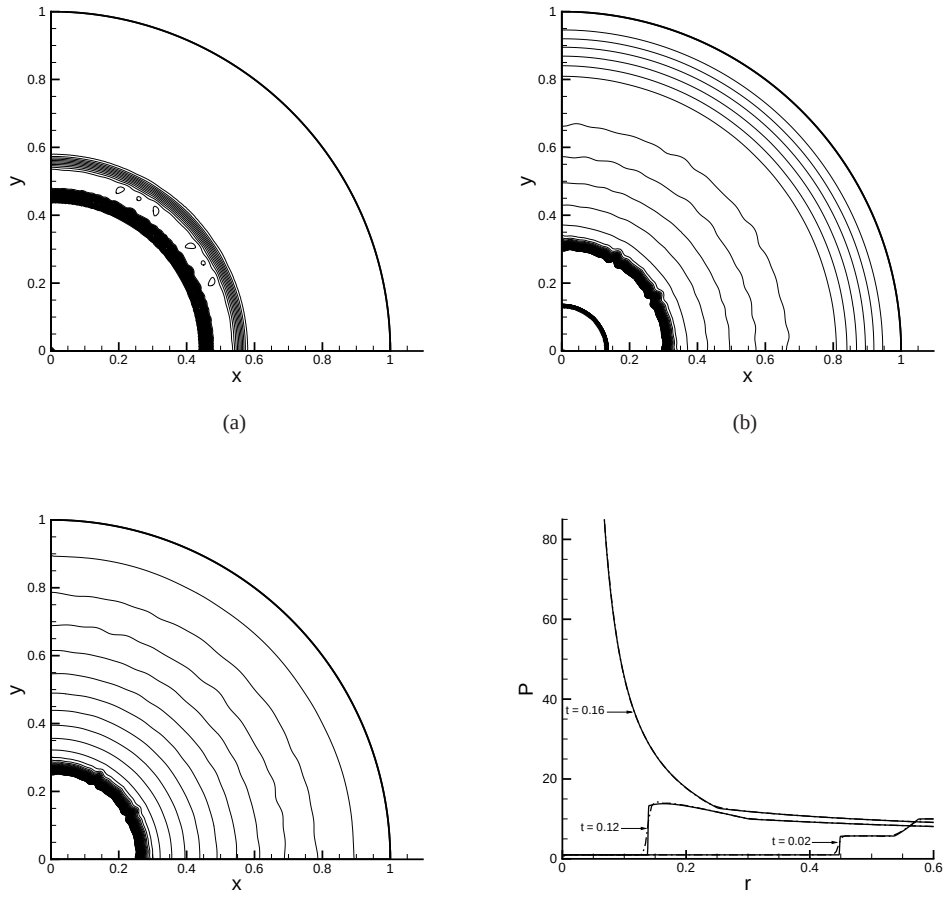

Figure 4: Density isoline for the implosion problem: (a) $t = 0.02$; (b) $t = 0.12$; (c) $t = 0.16$. Each isoline corresponds to a density difference of $\Delta\rho/\rho_{ref} = 0.03$. (d) Pressure signal along the $y = 0$ axis at the same time levels: the solid line is the reference one-dimensional solutions, the dot-dashed line is the bi-dimensional solution.

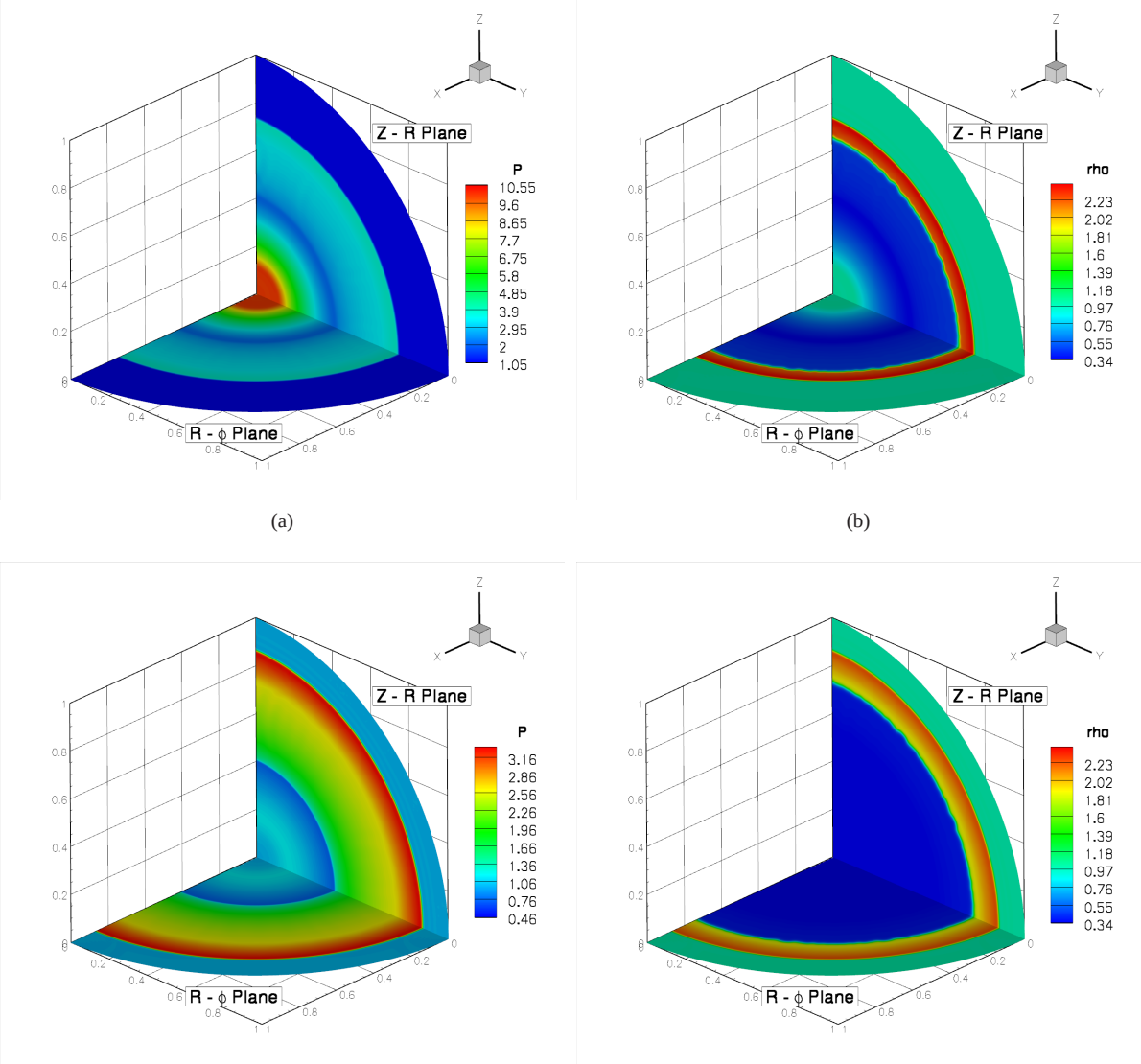

(a) (b)

(c) (d)

Figure 5: Pressure (a), (c) and density à (b), (d) contours for the explosion problem at two different time levels: $t = 0.1$ first row, $t = 0.16$ second row. On the horizontal plane is represented the solution of the bi-dimensional spherical problem on the r–ϕ plane, while on the vertical plane is represented the solution of the cylindrical axisymmetric problem on the Z–R plane.

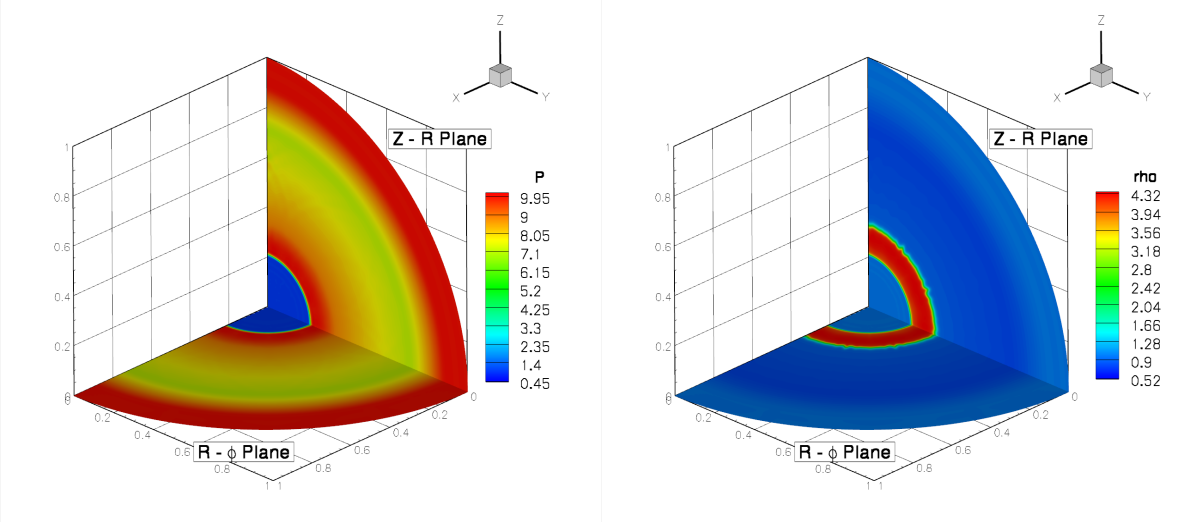

(a) (b)

(c) (d)

Figure 6: Pressure (a), (c) and density à (b), (d) contours for the implosion problem at two different time levels: $t = 0.1$ first row, $t = 0.16$ second row. On the horizontal plane is represented the solution of the bidimensional spherical problem on the r–ϕ plane, while on the vertical plane is represented the solution of the cylindrical axisymmetric problem on the Z–R plane.

scheme is used to discretize the additional contributions to the flow equations due to the action of viscosity and thermal conductivity. In the present work, where only inviscid simulations are considered, the hybrid approach is limited to the finite volume metrics computations. Numerical results are presented for two-dimensional compressible flows. These are the numerical simulation of the explosion and implosion problems, in which an initial discontinuity in pressure results in the formation of a diverging and converging shock, respectively. The computed pressure and density profile agree fairly well with one-dimensional simulation in spherical symmetry over a very fine grid. The solutions obtained in spherical reference also agree fairly well with the corresponding solutions in a cylindrical reference where the axisymmetric condition has been used to simulate spherical explosions and implosions.

References

[1] L. I. Sedov, Similarity and dimensional methods in mechanics, Academic Press, 1959.
[2] L. Fezou, B. Stoufflet, A class of implicit upwind schemes for Euler simulations with unstructured meshes, J. Comput. Phys. 84 (1989) 174 – 206.
[3] P. Rostand, B. Stoufflet, Tvd schemes to compute compressible viscous flows on unstructured grids, in: Vieweg (Ed.), J. Ballmann, R. Jeltsch (Eds.), Nonlinear Hyperbolic Equations Theory, Computation Methods, and Applications, 1989.
[4] P. Arminjon, A. Madrane, A mixed finite volume/finite element method for 2-dimensional compressible navierstokes equations on unstructured grids., in: Birkhäuser (Ed.), M. Fey, R. Jeltsch (Eds.), Hyperbolic Problems Theory, Numerics, Applications, International Series of Numerical Mathematics, vol. 129, 1998.
[5] C. Debiez, A. Dervieux, K. Mer, B. Nkonga, Computation of unsteady flows with mixed finite volume/finite element upwind methods, Numer. Meth. Fluids 27 (1998) 193–206.
[6] V. Selmin, The node-centred finite volume approach: bridge between finite differences and finite elements, Comp. Meth. Appl. Mech. Engng. 102 (1993) 107 – 138.
[7] L. Z. H. B. Chen, E. Panarella, Stability of imploding spherical shock waves, Journal of Fusion Energy 14 (1995) 389–392.
[8] V. Selmin, L. Formaggia, Unified construction of finite element and finite volume discretizations for compressible flows, Int. J. Numer. Meth. Eng. 39 (1996) 1 – 32.
[9] A. Guardone, L. Vigevano, Finite element/volume solution to axisymmetric conservation laws, J. Comput. Phys. 224 (2) (2007) 489 – 518.
[10] D. De Santis, G. Geraci, A. Guardone, Equivalence conditions for finite volume/element discretizations in cylindrical coordinates., V European Conference on Computational Fluid Dynamics ECCOMAS CFD 2010, 2010.
[11] A. Guardone, D. De Santis, G. Geraci, M. Pasta, On the relation between finite element and finite volume schemes for compressible flows with cylindrical and spherical symmetry, J. Comput. Phys. 230 (2010) 680–694.
[12] J. Donea, A. Huerta, Finite Element Methods for Flow Problems, Wiley, New York, 2002.
[13] R. J. LeVeque, Finite volume methods for conservation laws and hyperbolic systems, Cambridge University Press, 2002.
[14] A. Harten, J. M. Hyman, Self adjusting grid methods for one-dimensional hyperbolic conservation laws, J. Comput. Phys. 50 (1983) 253–269.
[15] B. van Leer, Towards the ultimate conservative difference scheme II. Monotonicity and conservation combined in a second order scheme, J. Comput. Phys. 14 (1974) 361 – 370.
[16] V. Venkatakrishnan, D. J. Mavriplis, Implicit method for the computation of unsteady flows on unstructured grids, Tech. rep. (1995).
[17] S. Rebay, Efficient unstructured mesh generation by means of of Delaunay triangulation and Browyer-Watson algorithm., J. Comput. Phys. 106 (1993) 125–138.

Appendix A. Node-pair finite element for a scalar conservation law

In this appendix, the following two identities are demonstrated, namely

$$\sum_{k\in\mathcal{N}_i} \boldsymbol{f}_k^{\circledcirc} \cdot \int_{\Omega_{ik}} r \sin\theta \varphi_k \boldsymbol{\nabla}^{\circledcirc} \varphi_i = \sum_{k\in\mathcal{N}_i,\neq} \left(\frac{\boldsymbol{f}_k^{\circledcirc} + \boldsymbol{f}_i^{\circledcirc}}{2} \cdot \boldsymbol{\eta}_{ik}^{\circledcirc} - \frac{\boldsymbol{f}_k^{\circledcirc} - \boldsymbol{f}_i^{\circledcirc}}{2} \cdot \boldsymbol{\zeta}_{ik}^{\circledcirc} \right) + \sum_{k\in\mathcal{N}_i,\neq} \frac{\boldsymbol{f}_k^{\circledcirc} - \boldsymbol{f}_i^{\circledcirc}}{2} \cdot \boldsymbol{\chi}_{ik}^{\circledcirc} \tag{A.1}$$

and

$$\sum_{k\in\mathcal{N}_i} \boldsymbol{f}_k^{\circledcirc} \cdot \int_{\partial\Omega_{ik}^{\partial}} r \sin\theta \varphi_i \varphi_k \boldsymbol{n}^{\circledcirc} = \sum_{k\in\mathcal{N}_{i,\neq}^{\partial}} (\boldsymbol{f}_k^{\circledcirc} - \boldsymbol{f}_i^{\circledcirc}) \cdot \boldsymbol{\chi}_{ik}^{\circledcirc} - \boldsymbol{f}_i^{\circledcirc} \cdot \boldsymbol{\xi}_i^{\circledcirc}, \tag{A.2}$$

which together allow to recast the discrete Bubnov-Galekin equation (3) in its node-pair counterpart (4).

The proof of the identity (A.1) is considered first. The integral on the left hand side of the Eq. (A.1) is assembled considering the contributions coming from each element e in the mesh, exploiting the local support property of the shape functions, as follows

$$\sum_{k\in\mathcal{N}_i} \boldsymbol{f}_k^{\circledcirc} \cdot \int_{\Omega_{ik}} r \sin\theta \varphi_k \boldsymbol{\nabla}^{\circledcirc} \varphi_i = \sum_{e\in\mathcal{E}_i} \sum_{k\in\mathcal{N}^e} \boldsymbol{f}_k^{\circledcirc} \cdot \int_{\Omega^e} r \sin\theta \varphi_k \boldsymbol{\nabla}^{\circledcirc} \varphi_i, \tag{A.3}$$

where $\mathcal{E}_i$ is the set of the elements having the node i in common and $\mathcal{N}^e$ is the set of the nodes of element e. The first summation on the right-hand side is limited to the elements contained in the support Ω_i of node i, which are the only ones to give a nonzero contribution to integrals containing the function φ_i. Note that $\Omega_i = \bigcup_{e\in\mathcal{E}_i} \Omega^e$. Considering now the following identity from the Gauss theorem

$$\int_{\Omega^e} \boldsymbol{\nabla}^\circ(r\sin\theta\varphi_i\varphi_k)\, d\Omega^\circ = \int_{\partial\Omega^e} r\sin\theta\varphi_i\varphi_k \boldsymbol{n}^\circ\, d\partial\Omega^\circ,$$

which allows to write

$$\int_{\Omega^e} r\sin\theta\varphi_k\boldsymbol{\nabla}^\circ\varphi_i = -\int_{\Omega^e} r\sin\theta\varphi_i\boldsymbol{\nabla}^\circ\varphi_k - \int_{\Omega^e}\varphi_i\varphi_k\boldsymbol{\nabla}^\circ(r\sin\theta) + \int_{\partial\Omega^e} r\sin\theta\varphi_i\varphi_k\boldsymbol{n}^\circ. \tag{A.4}$$

Thanks to the previous relation one deduces

$$\begin{aligned}\int_{\Omega^e} r\sin\theta\varphi_k\boldsymbol{\nabla}^\circ\varphi_i &= \frac{1}{2}\int_{\Omega^e} r\sin\theta\varphi_k\boldsymbol{\nabla}^\circ\varphi_i + \frac{1}{2}\int_{\Omega^e} r\sin\theta\varphi_k\boldsymbol{\nabla}^\circ\varphi_i \\ &= \frac{1}{2}\int_{\Omega^e} r\sin\theta\varphi_k\boldsymbol{\nabla}^\circ\varphi_i + \frac{1}{2}\left(-\int_{\Omega^e} r\sin\theta\varphi_i\boldsymbol{\nabla}^\circ\varphi_k - \int_{\Omega^e}\varphi_i\varphi_k\boldsymbol{\nabla}^\circ(r\sin\theta) + \int_{\partial\Omega^e} r\sin\theta\varphi_i\varphi_k\boldsymbol{n}^\circ\right) \\ &= -\frac{1}{2}\boldsymbol{\eta}_{ik}^{e,\circ} - \frac{1}{2}\int_{\Omega^e}\varphi_i\varphi_k\boldsymbol{\nabla}^\circ(r\sin\theta) + \frac{1}{2}\int_{\partial\Omega^e} r\sin\theta\varphi_i\varphi_k\boldsymbol{n}^\circ,\end{aligned} \tag{A.5}$$

where in the last equality has been introduced the elemental contributions $\boldsymbol{\eta}_{ik}^{e,\circ}$ of the element e to the vector $\boldsymbol{\eta}_{ik}^\circ$

$$\boldsymbol{\eta}_{ik}^{e,\circ} \stackrel{\text{def}}{=} \int_{\Omega_{ik}\cap\Omega^e} r\sin\theta(\varphi_i\boldsymbol{\nabla}^\circ\varphi_k - \varphi_k\boldsymbol{\nabla}^\circ\varphi_i),$$

such that $\boldsymbol{\eta}_{ik}^\circ = \sum_{e\in(\mathcal{E}_i\cap\mathcal{E}_k)} \boldsymbol{\eta}_{ik}^{e,\circ}$. By the relation (A.5), the integral (A.3) becomes

$$\sum_{k\in\mathcal{N}_i} \boldsymbol{f}_k^\circ \cdot \int_{\Omega_{ik}} R\varphi_k\boldsymbol{\nabla}^\circ\varphi_i = -\sum_{e\in\mathcal{E}_i}\sum_{k\in\mathcal{N}^e} \boldsymbol{f}_k^\circ \cdot \left(\frac{1}{2}\boldsymbol{\eta}_{ik}^{e,\circ} + \frac{1}{2}\int_{\Omega^e}\varphi_i\varphi_k - \frac{1}{2}\int_{\partial\Omega^e} R\varphi_i\varphi_k\boldsymbol{n}^\circ\right). \tag{A.6}$$

On the other hand, from the Eq. (A.5) follows also that

$$\boldsymbol{\eta}_{ik}^{e,\circ} = -2\int_{\Omega^e} R\varphi_k\boldsymbol{\nabla}^\circ\varphi_i - \int_{\Omega^e}\varphi_i\varphi_k\boldsymbol{\nabla}^\circ(r\sin\theta) + \int_{\partial\Omega^e} R\varphi_i\varphi_k\boldsymbol{n}^\circ,$$

which can be recast, using the equation (A.4), as

$$\boldsymbol{\eta}_{ik}^{e,\circ} = 2\int_{\Omega^e} R\varphi_i\boldsymbol{\nabla}^\circ\varphi_k + \int_{\Omega^e}\varphi_i\varphi_k\boldsymbol{\nabla}^\circ(r\sin\theta) - \int_{\partial\Omega^e} R\varphi_i\varphi_k\boldsymbol{n}^\circ.$$

Summing up the last relation for all the nodes k belonging to the element Ω^e and using the fact that $\sum_{k\in\mathcal{N}^e}\boldsymbol{\nabla}^\circ\varphi_k(\boldsymbol{x}^\circ) = \boldsymbol{0}, \forall \boldsymbol{x}^\circ \in \Omega^e$, one obtains

$$\sum_{k\in\mathcal{N}^e}\left(\boldsymbol{\eta}_{ik}^{e,\circ} - \int_{\Omega^e}\varphi_i\varphi_k\boldsymbol{\nabla}^\circ(r\sin\theta) + \int_{\partial\Omega^e} R\varphi_i\varphi_k\boldsymbol{n}^\circ\right) = \boldsymbol{0}. \tag{A.7}$$

Summing up the previous relation for all the elements belonging to $\mathcal{E}_i$ and multiplying by the vector $\boldsymbol{f}_i^\circ$, follows that

$$\sum_{e\in\mathcal{E}_i}\sum_{k\in\mathcal{N}^e} \boldsymbol{f}_i^\circ \cdot \left(\boldsymbol{\eta}_{ik}^{e,\circ} - \int_{\Omega^e}\varphi_i\varphi_k\boldsymbol{\nabla}^\circ(r\sin\theta) + \int_{\partial\Omega^e} R\varphi_i\varphi_k\boldsymbol{n}^\circ\right) = \boldsymbol{0}.$$

Multiplying this relation by $1/2$ and adding it to the right hand side of (A.6) one has

$$\begin{aligned}\sum_{k\in\mathcal{N}_i} \boldsymbol{f}_k^\circ \cdot \int_{\Omega_{ik}} R\varphi_k\boldsymbol{\nabla}^\circ\varphi_i = &-\sum_{e\in\mathcal{E}_i}\sum_{k\in\mathcal{N}^e}\left(\frac{\boldsymbol{f}_k^\circ + \boldsymbol{f}_i^\circ}{2}\cdot\boldsymbol{\eta}_{ik}^{e,\circ} + \frac{\boldsymbol{f}_k^\circ - \boldsymbol{f}_i^\circ}{2}\cdot\int_{\Omega^e}\varphi_i\varphi_k\boldsymbol{\nabla}^\circ(r\sin\theta)\right) \\ &+ \sum_{e\in\mathcal{E}_i}\sum_{k\in\mathcal{N}^e}\frac{\boldsymbol{f}_k^\circ - \boldsymbol{f}_i^\circ}{2}\cdot\int_{\partial\Omega^e} R\varphi_i\varphi_k\boldsymbol{n}^\circ.\end{aligned}$$

By recalling that $\boldsymbol{\eta}_{ik}^{e,\circ} = \mathbf{0}$ for $e \notin (\mathcal{E}_i \cap \mathcal{E}_k)$, that $\boldsymbol{\eta}_{ik}^{\circ} = \sum_{e\in(\mathcal{E}_i\cap\mathcal{E}_k)} \boldsymbol{\eta}_{ik}^{e,\circ}$ and that $\boldsymbol{\eta}_{ii}^{\varnothing} = \mathbf{0}$, the right hand side of the last equation can be written as

$$\sum_{k\in\mathcal{N}_i} \boldsymbol{f}_k^{\circ} \cdot \int_{\Omega_{ik}} R\varphi_k \boldsymbol{\nabla}^{\circ}\varphi_i = -\sum_{k\in\mathcal{N}_{i,\neq}} \left(\frac{\boldsymbol{f}_k^{\circ} + \boldsymbol{f}_i^{\circ}}{2} \cdot \boldsymbol{\eta}_{ik}^{\circ} + \frac{\boldsymbol{f}_k^{\circ} - \boldsymbol{f}_i^{\circ}}{2} \cdot \boldsymbol{\zeta}_{ik}^{\circ} \right) + \sum_{k\in\mathcal{N}_{i,\neq}^{\partial}} \frac{\boldsymbol{f}_k^{\circ} - \boldsymbol{f}_i^{\circ}}{2} \cdot \int_{\partial\Omega_{ik}^{\partial}} R\varphi_i\varphi_k \boldsymbol{n}^{\circ},$$

that is the relation (A.1).

Considering now the proof of the identity (A.2), in the left hand side of (A.2) the contribute of the node i is put into evidence, namely

$$\sum_{k\in\mathcal{N}_i^{\partial}} \boldsymbol{f}_k^{\circ} \cdot \int_{\partial\Omega_{ik}^{\partial}} R\varphi_i\varphi_k \boldsymbol{n}^{\circ} = \sum_{k\in\mathcal{N}_{i,\neq}^{\partial}} \boldsymbol{f}_k^{\circ} \cdot \int_{\partial\Omega_{ik}^{\partial}} R\varphi_i\varphi_k \boldsymbol{n}^{\circ} + \boldsymbol{f}_i^{\circ} \cdot \int_{\partial\Omega_{ik}^{\partial}} R\varphi_i\varphi_i \boldsymbol{n}^{\circ}.$$

The quantity

$$\sum_{k\in\mathcal{N}_{i,\neq}^{\partial}} \boldsymbol{f}_i^{\circ} \cdot \int_{\partial\Omega_{ik}^{\partial}} R\varphi_i\varphi_k \boldsymbol{n}^{\circ},$$

is now added and subtracted from the right hand side to obtain

$$\sum_{k\in\mathcal{N}_i^{\partial}} \boldsymbol{f}_k^{\circ} \cdot \int_{\partial\Omega_{ik}^{\partial}} R\varphi_i\varphi_k \boldsymbol{n}^{\circ} = \sum_{k\in\mathcal{N}_{i,\neq}^{\partial}} (\boldsymbol{f}_k^{\circ} - \boldsymbol{f}_i^{\circ}) \cdot \int_{\partial\Omega_{ik}^{\partial}} R\varphi_i\varphi_k \boldsymbol{n}^{\circ} + \boldsymbol{f}_i^{\circ} \cdot \sum_{k\in\mathcal{N}_i^{\partial}} \int_{\partial\Omega_{ik}^{\partial}} R\varphi_i\varphi_k \boldsymbol{n}^{\circ}.$$

By recalling that $\sum_{k\in\mathcal{N}_e} \varphi_k(\boldsymbol{x}^{\circ}) = 1, \boldsymbol{x}^{\circ} \in \Omega^e, \forall e \in \mathcal{E}$, one has

$$\begin{aligned}\sum_{k\in\mathcal{N}_i^{\partial}} \boldsymbol{f}_k^{\circ} \cdot \int_{\partial\Omega_{ik}^{\partial}} R\varphi_i\varphi_k \boldsymbol{n}^{\circ} &= \sum_{k\in\mathcal{N}_{i,\neq}^{\partial}} (\boldsymbol{f}_k^{\circ} - \boldsymbol{f}_i^{\circ}) \cdot \int_{\partial\Omega_{ik}^{\partial}} R\varphi_i\varphi_k \boldsymbol{n}^{\circ} + \boldsymbol{f}_i^{\circ} \cdot \int_{\partial\Omega_i^{\partial}} R\varphi_i \boldsymbol{n}^{\circ} \\ &= \sum_{k\in\mathcal{N}_{i,\neq}^{\partial}} (\boldsymbol{f}_k^{\circ} - \boldsymbol{f}_i^{\circ}) \cdot \boldsymbol{\chi}_{ik}^{\circ} + \boldsymbol{f}_i^{\circ} \cdot \boldsymbol{\xi}_i^{\circ},\end{aligned}$$

which is the relation (A.2). Using the relations (A.1), (A.2) is possible to write (2) as follow

$$\begin{aligned}\sum_{k\in\mathcal{N}_i} M_{ik}^{\circ} \frac{du_k}{dt} = &-\sum_{k\in\mathcal{N}_i,\neq} \left(\frac{\boldsymbol{f}_k^{\circ} + \boldsymbol{f}_i^{\circ}}{2} \cdot \boldsymbol{\eta}_{ik}^{\circ} + \frac{\boldsymbol{f}_k^{\circ} - \boldsymbol{f}_i^{\circ}}{2} \cdot \boldsymbol{\zeta}_{ik}^{\circ} \right) + \sum_{k\in\mathcal{N}_i} \boldsymbol{f}_k^{\circ} \cdot \int_{\Omega_{ik}} \varphi_i\varphi_k \boldsymbol{\nabla}^{\circ}(r\sin\theta) \\ &- \sum_{k\in\mathcal{N}_{i,\neq}^{\partial}} \frac{\boldsymbol{f}_k^{\circ} - \boldsymbol{f}_i^{\circ}}{2} \cdot \boldsymbol{\chi}_{ik}^{\circ} - \boldsymbol{f}_i^{\circ} \cdot \boldsymbol{\xi}_i^{\circ},\end{aligned} \tag{A.8}$$

with the metric quantities defined in (5). In the previous relation is necessary to write in node-pair form also the second term on the right hand side. By recalling that

$$\sum_{k\in\mathcal{N}_i} \boldsymbol{f}_k^{\circ} \cdot \int_{\Omega_{ik}} \varphi_i\varphi_k \boldsymbol{\nabla}^{\circ}(r\sin\theta) = \sum_{k\in\mathcal{N}_{i,\neq}} \boldsymbol{f}_k^{\circ} \cdot \int_{\Omega_{ik}} \varphi_i\varphi_k \boldsymbol{\nabla}^{\circ}(r\sin\theta) + \boldsymbol{f}_i^{\circ} \cdot \int_{\Omega_{ik}} \varphi_i\varphi_k \boldsymbol{\nabla}^{\circ}(r\sin\theta),$$

by adding and subtracting to the previous relation the following quantity

$$\sum_{k\in\mathcal{N}_{i,\neq}} \boldsymbol{f}_i^{\circ} \cdot \int_{\Omega_{ik}} \varphi_i\varphi_k \boldsymbol{\nabla}^{\circ}(r\sin\theta),$$

one has

$$\begin{aligned}\sum_{k\in\mathcal{N}_i} \boldsymbol{f}_k^{\circ}\cdot\int_{\Omega_{ik}}\varphi_i\varphi_k\boldsymbol{\nabla}^{\circ}(r\sin\theta) &= \sum_{k\in\mathcal{N}_{i,\neq}}(\boldsymbol{f}_k^{\circ}-\boldsymbol{f}_i^{\circ})\cdot\int_{\Omega_{ik}}\varphi_i\varphi_k\boldsymbol{\nabla}^{\circ}(r\sin\theta)+\sum_{k\in\mathcal{N}_i}\boldsymbol{f}_i^{\circ}\cdot\int_{\Omega_{ik}}\varphi_i\varphi_k\boldsymbol{\nabla}^{\circ}(r\sin\theta)\\ &= \sum_{k\in\mathcal{N}_{i,\neq}}(\boldsymbol{f}_k^{\circ}-\boldsymbol{f}_i^{\circ})\cdot\int_{\Omega_{ik}}\varphi_i\varphi_k\boldsymbol{\nabla}^{\circ}(r\sin\theta)+\boldsymbol{f}_i^{\circ}\cdot\int_{\Omega_{ik}}\varphi_i\boldsymbol{\nabla}^{\circ}(r\sin\theta)\\ &= \sum_{k\in\mathcal{N}_{i,\neq}}(\boldsymbol{f}_k^{\circ}-\boldsymbol{f}_i^{\circ})\cdot\int_{\Omega_{ik}}\varphi_i\varphi_k\boldsymbol{\nabla}^{\circ}(r\sin\theta)+\boldsymbol{f}_i^{\circ}\cdot\widehat{\boldsymbol{L}}_i^{\circ}.\end{aligned} \tag{A.9}$$

by substituting this relation into the (A.8) one has the node-pair FE discretization of the scalar equation (1)

$$\begin{aligned}L_i^{\circ}\frac{du_i}{dt} = &-\sum_{k\in\mathcal{N}_{i,\neq}}\left(\frac{\boldsymbol{f}_k^{\circ}+\boldsymbol{f}_i^{\circ}}{2}\cdot\boldsymbol{\eta}_{ik}^{\circ}-\frac{\boldsymbol{f}_k^{\circ}-\boldsymbol{f}_i^{\circ}}{2}\cdot\boldsymbol{\zeta}_{ik}^{\circ}\right)+\boldsymbol{f}_i^{\circ}\cdot\widehat{\boldsymbol{L}}_i^{\circ}\\ &-\sum_{k\in\mathcal{N}_{i,\neq}^{\theta}}\frac{\boldsymbol{f}_k^{\circ}-\boldsymbol{f}_i^{\circ}}{2}\cdot\boldsymbol{\chi}_{ik}^{\circ}-\boldsymbol{f}_i^{\circ}\cdot\boldsymbol{\xi}_i^{\circ},\end{aligned} \tag{A.10}$$

where the mass matrix has been lumped

$$\sum_{k\in\mathcal{N}_i} M_{ik}^{\circ}\frac{du_i}{dt}\simeq L_i^{\circ}\frac{du_i}{dt},$$

with $L_i^{\circ}=\sum_{k\in\mathcal{N}_i}M_{ik}^{\circ}$.